JOURNAL OF GUIDANCE, CONTROL, AND DYNAMICS
Vol. 29, No. 2, March–April 2006

Design of Autoland Controller Functions with Multiobjective Optimization

Gertjan Looye* and Hans-Dieter Joos†
German Aerospace Center, DLR-Oberpfaffenhofen, 82234 Wessling, Germany

The application of multiobjective optimization to the design of longitudinal automatic-landing control laws for a civil aircraft is discussed. The control laws consist of a stability and command augmentation, a speed/flight path tracking, a glide-slope guidance, and a flare function. Multiobjective optimization is used to synthesize the free parameters in these controller functions. Performance criteria are thereby computed from linear as well as nonlinear analysis. Robustness to uncertain and varying parameters is addressed via linear robustness criteria and via statistical criteria computed from online Monte Carlo analysis. For each controller function, an optimization problem setup is defined. Starting with the inner loops, the synthesis is sequentially expanded with each of these setups, eventually leading to simultaneous optimization of all controller functions. In this way, dynamic interactions between controller components are accounted for, and inner loops can be compromised such that these can be used in combination with different outer loop functions. This reduces controller complexity while providing good overall control system performance.

I. Introduction

THE development of automatic landing (autoland) control laws for civil aircraft is a demanding task, because high safety standards have to be met before operational use under most adverse weather and visibility conditions (e.g., category III[1]) is allowed. The landing mission, consisting of glide-slope tracking and flare/runway alignment shortly before touchdown, is relatively straightforward. However, the autoland design task is complicated by the large amount of varying and uncertain parameters. First, aircraft loading and configuration parameters may vary for each landing case. Second, environmental parameters, such as runway, approach terrain, instrument landing system (ILS), atmosphere, and wind characteristics, are different for each landing. Some of these parameters are illustrated in Fig. 1. For certification, autoland performance under varying aircraft and environment parameters has to be demonstrated via extensive Monte Carlo (MC) analysis, augmented with flight-test validation.[1] The control designer also has to account for uncertain parameters in the aircraft-design model to cover differences with the actual aircraft or even with the high-fidelity and flight-test-validated model used for final Monte Carlo assessment.[2]

Autoland control laws consist of functions for glide slope and localizer hold, flare and runway alignment (in case of cross wind), and inner loops for stability and command augmentation. The design of these functions relies heavily on engineering skills and experience of the designer(s) and may involve considerable trial and error to tune the controller parameters to meet design specifications. Important problems are the large number of design criteria that have to be addressed in the face of the aforementioned varying and uncertain model parameters, as well as the criteria themselves. Typical autoland design requirements, for example regarding touchdown performance, do not always translate easily into computational criteria that can be handled by commonly used controller synthesis methods. As a consequence, the designer has to manually iterate between assessing autoland performance and adjusting controller (synthesis) parameters.

In this paper, these problems are addressed by the application of a flight-control-law design process that is based on multiobjective optimization.[3,4] This approach involves optimization of free design parameters in a predefined controller structure (e.g., gains, filter time constants) or in a controller synthesis setup (e.g., Q and R weighting matrices in LQ synthesis) with respect to a possibly large set of computational criteria and constraints. An important advantage is that these criteria and constraints may be directly derived from engineering design specifications and computed from linear and/or nonlinear analysis of the closed-loop system. For example, touchdown velocity and distance, computed from a nonlinear automatic-landing simulation, are valid synthesis criteria. Relative importance of criteria is expressed via scaling.

Features of multiobjective optimization are exploited to address robustness to varying landing and aircraft parameters and uncertainty. Stability robustness to aircraft model uncertainty is addressed via gain and phase margins as design criteria. As part of the certification effort, MC analysis is required to prove that the probability of exceeding bounds on specific landing parameters (e.g., maximum sink rate at touchdown) under varying environment and aircraft parameters and disturbances is below a certain level. It is shown that these stochastic measures can be directly incorporated as optimization criteria, providing an effective means to address robustness to varying aircraft and environmental parameters. A similar principle for robust multiobjective tuning of control laws was proposed by Schy and Giesy,[5] who used a linear approach to compute stochastic properties of performance measures. In this work, online MC analysis is performed to compute risk-based criteria, providing a direct link with certification requirements and allowing additional criteria to be computed from individual simulations.

The actual optimization problem is formulated as minimizing the maximum over all scaled criteria, under the specified inequality or equality constraints.[6] This so-called min–max approach allows the designer to steer compromise solutions between conflicting criteria by adjusting their scalings. The applied methodology was developed by Kreisselmeier and Steinhauser and has been implemented in the computer-aided control-system design tool MOPS (multiobjective parameter synthesis),[7] developed at the DLR Institute of Robotics and Mechatronics. A similar min–max optimization approach was proposed by Schy and Giesy[5] and is also applied in the Control Designer's Unified Interface (CONDUIT®) by Tischler et al.[8]

Presented as Paper 2002-4666 at the AIAA Guidance, Navigation, and Control Conference, Monterey, CA, 5–8 August 2002; received 5 March 2004; revision received 8 October 2004; accepted for publication 5 May 2005.

*Research Engineer, Institute of Robotics and Mechatronics, Control Design Engineering Department; Gertjan.Looye@DLR.de.

†Research Engineer, Institute of Robotics and Mechatronics, Control Design Engineering Department; Dieter.Joos@DLR.de.

The optimization approach makes it possible to simultaneously tune all design parameters in all control-law functions. This saves manual iterations to harmonize performance of individual functions and allows controller complexity to be reduced, because one set of inner-loop functions may be tuned to work in combination with different outer-loop functions. However, performing this optimization in one shot is impractical. For the designer it becomes difficult to keep track of the large amount of criteria and design parameters (making it hard to decide if and where the controller structure needs to be enhanced), to recognize and adjust conflicting criteria, and so forth. For this reason, a stepwise tuning strategy is proposed. Inner-loop functions are tuned first, and then the optimization task is expanded step by step with the outer-loop functions, eventually leading to simultaneous optimization of all tuning parameters in all functions. The designer can thus concentrate on one function at a time, but eventually the optimization addresses the integrated system. Because tuning parameter values resulting from one optimization provide starting values for the next, higly efficient local optimization algorithms in general work well.

In this paper the design of the longitudinal part of an autoland system for a small passenger aircraft is discussed. More details on the lateral modes can be found in Ref. 4. An in-depth discussion on robust tuning of the lateral inner loops is presented in Ref. 9.

This paper is structured as follows: In Sec. II the aircraft model is briefly described. In Sec. III the applied design process is discussed. The individual steps in this process are described in Sec. IV (controller architecture), Sec. V (optimization setups for the controller functions), Secs. VI and VII (the optimization strategy and optimization problem formulation), and in Sec. VIII (analysis of design results). Finally, conclusions are drawn in Sec. IX.

II. Aircraft Model

The aircraft is a VFW-614 (∼30 passengers) called ATTAS (advanced technologies testing aircraft system), which has been configured as DLR's fly-by-wire test bed.[10]

The model is based on the Newton–Euler equations of motion for a rigid body.[11] The aerodynamics are valid for the landing configuration and include unsteady effects, ground effect, and interaction with the engine exhaust. Aerodynamic coefficients as well as the moments of inertia have tolerances between 10% and 30%. These tolerances were provided with the aircraft model. Ground-effect coefficients and dynamic stability derivatives have the highest level of uncertainty. For example, the tolerance on the derivative of the aerodynamic pitching moment coefficient C_m with respect to the pitch rate q is written as

$$C_{m_q} = C_{m_{q0}}\left(1 + \Delta C_{m_q}\right) \tag{1}$$

where $C_{m_{q0}}$ is the nominal value and ΔC_{m_q} is the tolerance: $-0.3 \le \Delta C_{m_q} \le 0.3$. The vector containing all uncertain parameter tolerances in the aircraft model is $\boldsymbol{p}_u$.

The available controls are ailerons δ_A, elevator δ_E, rudder δ_R, and engine throttle settings $\delta_{\mathrm{TH}1,2}$. The tail plane angle of incidence δ_T is used for trimming. The control surface actuators are linear, but rate and position limited. The turbofan engine dynamics and thrust computation are nonlinear. The fuel-control unit shows backlash behavior, equivalent to several degrees of throttle input.

The wind model includes wind shear as present in the Earth's boundary layer, Dryden turbulence filters (as specified in Ref. 1), as well as additional parameterized wind-shear models. Parameterized models are included for the atmosphere, approach terrain, runway and ILS equipment characteristics. The environmental parameters are contained in the vector $\boldsymbol{p}_e$ (Fig. 1).

The model outputs are the measurements available to the control system: calibrated airspeed V_{cas}; true airspeed V_{tas}; ground speed V_g; body angular rates p, q, and r; attitude angles ϕ, θ, and ψ; load factors n_x, n_y, and n_z; track and flight path angles χ and γ; angle of attack α; vertical speed V_Z; deviations from the ILS beam ϵ_{LOC} (localizer); ϵ_{GS} (glide slope, both in mA); radio and barometric altitude H_{ra} and H_{baro}; and the mean fan-shaft speed of both engines N_1. The sensor models are linear, but the output signals are quantized. The signals N_1, ϵ_{LOC}, ϵ_{GS}, and α are corrupted with noise. Finally, parameters related to the aircraft configuration (e.g., the mass m and the center of gravity location x_{CG}) may be assumed known to the controller and are collected in the vector $\boldsymbol{p}_a$.

III. Applied Design Process

The design process as applied for the automatic landing control laws is depicted in Fig. 2. As a first step (A), the global architecture is defined. Detailed design of functions within this architecture is addressed in step B, involving detailed specification of the control-law structure and the formulation of function-specific computational

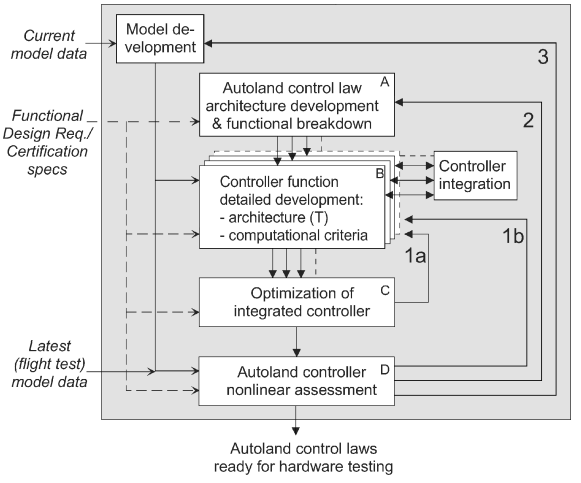

Fig. 2 Optimization-based autoland control laws design process.

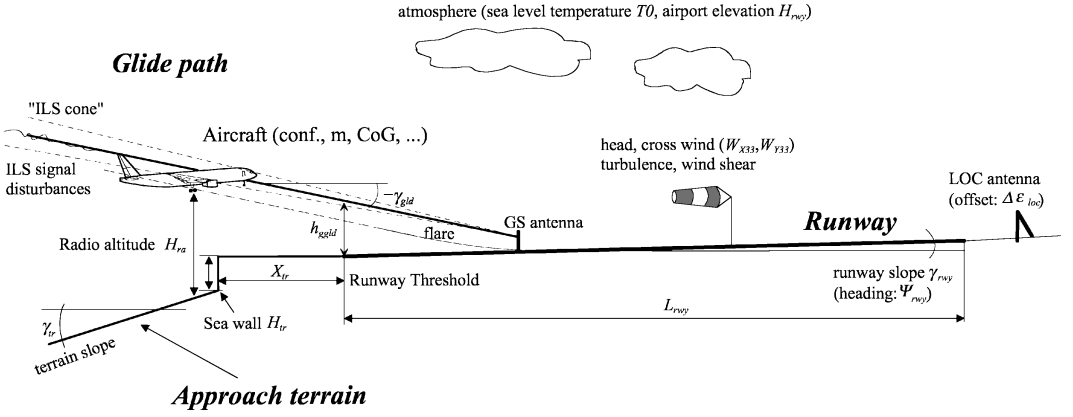

Fig. 1 Typical parameters and disturbances during a landing.

criteria. The controller structures are integrated into the autoland system, which, in combination with the aircraft model, can then be used for the closed-loop analysis required for criteria computation.

The actual optimization of the controller functions is performed in step C. Here the tuning strategy as sketched in Sec. I is applied, eventually allowing all controller components to be optimized simultaneously.

Performance and robustness of the resulting autoland system is assessed in step D of Fig. 2. The iteration loops 1a and 1b involve adjustments to computational criteria or component architectures, in case optimization or assessment results are not satisfactory or to further improve them. In case of severe shortcomings, the overall controller structure may have to be reconsidered (loop 2). Loop 3 may be required in case of major model updates. However, by explicitly addressing model uncertainty in the process, this loop may possibly be avoided.

IV. Controller Architecture

This section addresses step A (global architecture) and partially step B (detailed function architectures) in the design process in Fig. 2. The selected global structure for the autoland controller is depicted in Fig. 3. It has previously been applied to a large transport aircraft.[4] Three main loops can be identified, separated by dashed lines: stability and command augmentation (SCA), speed/path tracking (SPT), and guidance. Complexity of autopilot-control laws may be considerably reduced by implementing only one component for each function only. This is an important feature of the total energy control system (TECS), which is used as an SPT function: a single speed/path tracking control law can be used as the core of a complete set of longitudinal autopilot modes.[12,13] In this autoland architecture, the same principle is applied to the SCA function, which is used by all SPT functions. In this paper, only the design of the longitudinal controller functions is discussed. A brief description of each of the functions is given in the following subsections.

A. Inner Loops

The task of the inner loops is to improve stability and to achieve robust tracking of command variables (ϕ_c, θ_c, $\dot{\psi}_c$). The use of θ_c as inner-loop command variable allows for direct control over the pitch attitude dynamics. Especially during flare, these play an important role in pilot acceptance.

The inner loops were designed with nonlinear dynamic inversion (NDI).[14] Inverse model equations compensate the nonlinear aircraft dynamics, resulting in uniform and decoupled command responses, so that (manual) gain scheduling of the control laws is avoided. Note that in this way also known aircraft loading and configuration parameters ($\boldsymbol{p}_a$), provided to the controller, are automatically compensated for. A more detailed discussion on the inner loops can be found in Ref. 9.

The closed-loop dynamics are shaped using a linear outer-loop control law:

$$\nu_d = K_\theta(\theta_c - \theta) - K_q q \tag{2}$$

where ν_d is the pitch acceleration command to the NDI controller, θ_c is the commanded pitch attitude angle, and K_θ and K_q are constant gains.

B. Longitudinal Tracking and Glide Slope Mode

For longitudinal speed and flight-path tracking during the approach, TECS is used[13]; see Fig. 4. The TECS architecture offers pilot-like decoupled tracking of speed and flight-path angle commands. The input signals are air-mass-referenced flight-path angle $\gamma_a \approx -\dot{V}_Z/V_{\text{cas}}$ and filtered acceleration $\hat{\dot{V}}/g$. Here, TECS controls pitch attitude θ_c and thrust (per unit weight, $\delta T_c/W$). An inverse thrust map and an engine backlash compensation scheme (BLcomp) are used to generate appropriate throttle commands (Fig. 3). The gain K_F allows for shifting control priority to flight-path tracking. The speed loop is opened in case thrust saturates.

The feedback signal $\hat{\dot{V}}/g$ is obtained from complementarily filtering of the measured calibrated airspeed V_{cas} and the time derivative of the inertial speed $\dot{V}$ (computed from inertial reference signals), with time constant τ_V.[13] The acceleration error $\tilde{\dot{V}}_e/g$ is computed from proportional feedback of the calibrated airspeed:

$$\tilde{\dot{V}}_e = K_V(V_{\text{app}} - V_{\text{cas}}) - \hat{\dot{V}} \tag{3}$$

where V_{app} is the selected approach speed.

The flight-path angle error is computed in the glide slope (GS) mode[13]:

$$\gamma_e = \frac{1}{\hat{V}}\left[K_h \frac{1}{\tau_h s + 1}\Delta\tilde{h} - \hat{\dot{h}}\right] \tag{4}$$

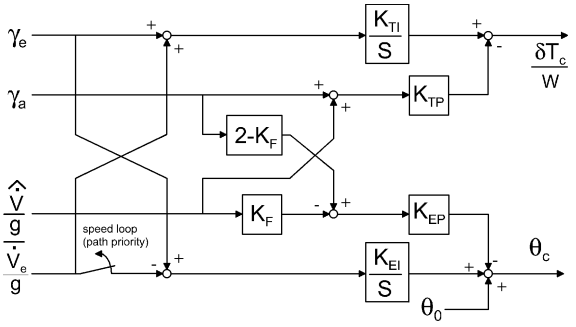

Fig. 4 TECS controller structure (subscript *e* denotes an error from a commanded value).

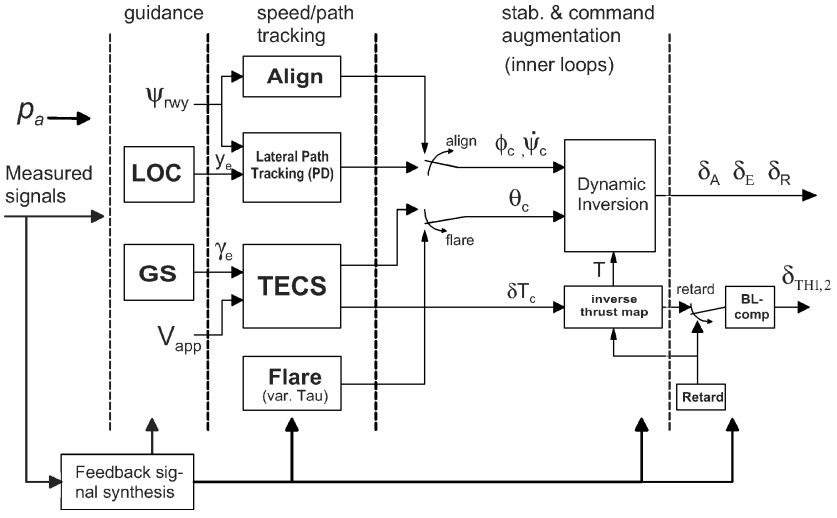

Fig. 3 Autoland controller architecture (for block inputs, only command and error signals shown).

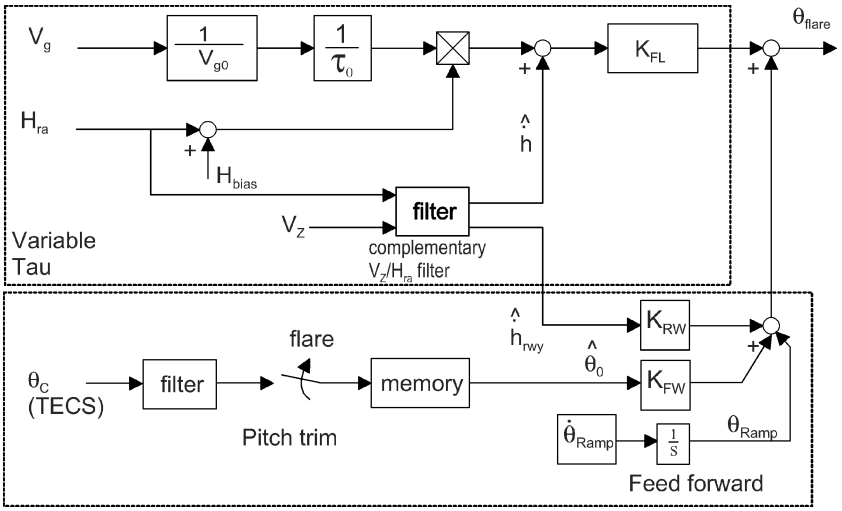

Fig. 5 Variable τ-based flare law architecture.

where $\hat{V}$ is a complementarily filtered speed signal and $\Delta\tilde{h}$ is the height error estimated from the glide slope signal, which is filtered with time constant τ_h to remove high-frequency signal noise. The estimated vertical speed with respect to the glide slope $\hat{\dot{h}}$ is obtained from complementarily filtering $\Delta\tilde{h}$ and inertial reference signals (time constant is $\tau_{\dot{h}}$).

C. Flare Law

For the flare law, the so-called variable tau principle[15] was chosen (Fig. 5). It features constant initiation height (H_{flare}) and low touchdown dispersion under varying wind conditions. A feedforward part is added consisting of a ramp command to increase pitch (θ_{Ramp}), as well as the mean TECS attitude command $\hat{\theta}_0$, multiplied by K_{FW} (obviously, the starting value for tuning is 1). The angle $\hat{\theta}_0$ is obtained by low-pass filtering θ_c commanded by TECS during the approach, and holding the value from flare initiation (Fig. 5).

The vertical speed $\hat{\dot{h}}$ is obtained by complementary filtering the radio altitude H_{ra} and V_Z, resulting in a runway referenced signal with low noise content. From the difference $\hat{\dot{h}} - (-V_Z)$ an additional feedforward command is generated via K_{RW}, anticipating a possible runway slope. During flare the throttles are retarded at a constant rate $\dot{\delta}_{\text{TH}_c}$ (proportional to the ground speed at flare initiation), such that these reach idle position at touchdown.

V. Optimization Problem Setups

This section addresses step B in the design process in Fig. 2. For each individual controller function, an optimization problem setup is defined. Such a setup includes properties of the free parameters in the controller structure, computational design criteria (including properties such as scaling, minimizing or inequality constraint, etc.) that apply to the specific function, as well as macros and models to compute these criteria. Visualization of analysis results is configured as well, allowing the designer to qualitatively monitor the design progress.

A. Stability and Command Augmentation (SCA)

The gains K_θ and K_q are tuning parameters for command shaping. If necessary, uncertain model parameters that also appear in the inverse model equations ($\boldsymbol{p}_u^*$) can be effectively used as additional tuning parameters to improve robustness.[9] The criteria for the longitudinal part of the NDI inner loop are listed in Table 1. Those based on simulation 1 are intended for command shaping, those on simulation 2 for disturbance rejection, and those based on linear analysis are intended to guarantee closed-loop stability (overall eigenvalues, including zero dynamics) and stability robustness to model uncertainty (e.g., time delays, unmodeled dynamics).

In multiobjective optimization, relative importance of criteria is expressed via scaling. Especially in cases of conflicting requirements, this gives the designer an effective means to make trade-offs and to set priorities. Scaled criteria have to be formulated such, that the objective is to minimize them, and that a value less than one is considered satisfactory.

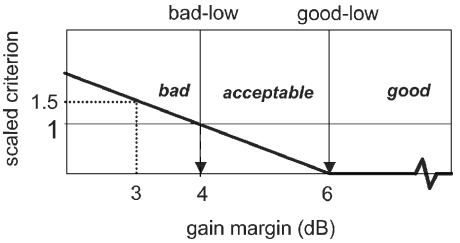

Fig. 6 Scaling of *gmAD* with good–bad values.

Table 1 Criteria for the SCA function[a]

Name	Description	Computation
	Simulation 1, step: $\theta_c = 5$ deg, no turbulence	
THrt	Rise time	—[a]
THos	Overshoot	—[a]
THcontr	δ_E Control activity	$\max_{t>1.3\,\text{s}}\{\lvert\dot{\delta}_E\rvert\}$
	Simulation 2, heavy turbulence	
THturb	Disturbance rejection	$(1/60)\int_{t=0}^{t=60}(\theta_c-\theta)^2 dt$
	Linear analysis	
gmAD	Gain margin at δ_E-act.	—[a]
pmAD	Phase margin at δ_E-act.	—[a]
gmST	Gain margin at θ-sens.	—[a]
pmST	Phase margin at θ-sens.	—[a]
DAMPdi	Min. damping (lon)	$\min\{\zeta_i\}$ (longitudinal)

[a]All computations: symmetrical horizontal flight; altitude = 1000 ft; nominal aircraft loading. Step times: $t_s = 1$ s. Rise time: Δt between 10% and 90% of command. Gain/phase margins: computed using margin-command.[16]

Criteria scaling can be performed by dividing each criterion by its demanded value:

$$\hat{c}_k(\boldsymbol{T}) = c_k(\boldsymbol{T})/d_k \tag{5}$$

where $c_k(\boldsymbol{T})$ and d_k are the computed value and demanded value of criterion k respectively and $\boldsymbol{T}$ denotes the current set of tuning parameters. Scaling can also be done using so-called good–bad values,[3] as is illustrated for *gmAD* in Fig. 6. The demand is that the gain margin is at least 4 dB (bad-low). Any value larger than 6 (good-low) is considered equally good and therefore scaled to 0. Below 6 dB, the scaled value increases linearly, such that a value of 1 is reached for the bad-low value of 4 dB. Any value between 4 and 6 dB is acceptable; any value lower than 4 dB is considered unacceptable (bad). As an example, if the gain margin is 3 dB, its scaled value equals 1.5. In the same fashion, good-high and bad-high

Table 2 Scalings of all optimization criteria[a]

Criterion, unit	Bad low	Good low	Good high	Bad high	Demand	Type
Longitudinal SCA criteria						
THrt, s	—	—	—	—	2.5	c
THos, −	—	—	—	—	0.05	c
THcontr, deg/s	—	—	—	—	12.0	m
THturb, deg^2	—	—	—	—	0.08	p
gmAD, −	—	—	4.0	6.0	1	m
pmAD, deg	—	—	40	60	1	c
gmST, −	—	—	4.0	6.0	1	m
pmST, deg	—	—	40	60	1	c
DAMPdi, −	—	—	0.5	0.7	1	c
Longitudinal SPT criteria						
GArt, s	—	—	—	—	16.0	c
GAos, −	—	—	—	—	0.1	c
GAst, deg	—	—	—	—	0.2	m
THcmd, deg/s	—	—	—	—	2.0	m
GAVA, m/s	—	—	—	—	0.5	m
VArt, s	—	—	—	—	20.0	c
VAos, −	—	—	—	—	0.10	c
VAst, m/s	—	—	—	—	0.5	m
dTHR, deg/s	—	—	—	—	0.15	m
VAGA, deg	—	—	—	—	1.0	m
NZturb, s^{-2}	—	—	—	—	0.007	p
THCturb, deg^2	—	—	—	—	0.167	p
THRturb, deg^2	—	—	—	—	5	p
Glide slope criteria						
GSrt, s	—	—	—	—	20	c
GSos, −	—	—	—	—	0.12	m
GSst, m	—	—	—	—	2	c
maxGSdev, mA	—	—	—	—	200	m
maxGSdev50, mA	—	—	—	—	200	m
meanGSdev, mA	—	—	—	—	1	m
maxTHEdev, deg	—	—	—	—	3	m
maxVCdev, m/s	—	—	—	—	8.0	m
Flare criteria						
XTDnom, m	360	380	400	420	1	m
VZTDnom, m/s	−3.0	−2.8	−2.4	−2.2	1	m
THgrad, rad/s	—	—	—	—	1	c
dHgrad, m/s	—	—	—	—	1	c
dDEmax, deg/s	—	—	—	—	10	c
meanHTP60, m	8	10	12	15	1	m
stdevHTP60, m	—	—	—	—	1.3	m
limHTP60, m	0	5	—	—	1	c
meanXTD, m	300	350	400	450	1	m
stdevXTD, m	—	—	—	—	75	m
limXTD, m	—	—	—	—	680	c
meanVZTD, m/s	−6	−4	−2	−1.5	1	m
stdevVZTD, m/s	—	—	—	—	1.4	m
limVZTD, m/s	—	—	—	—	3.1	c

[a]c = inequality constraint, m = minimize, p = passive.

values can be specified. It must be noted that the corner between the sloping line (<6 dB) and the horizontal line projecting criteria values to zero is (sharply) rounded using an exponential approximation to make sure the scaled criterion value remains smooth.

The scalings applied to the SCA criteria are given in the first part of Table 2 (*THrt*... *DAMPdi*). Some of the criteria are treated as inequality constraints [i.e., $\hat{c}_k(\boldsymbol{T}) \leq 1$]. For example, an overshoot of less than 5% is demanded. If this is satisfied, there is no point to further minimize this criterion, because this may unnecessarily go at the cost of rise time. The criterion *THturb* is passive: its value is computed at each iteration step for monitoring but is ignored by the optimizer. Of course, passive criteria may be activated any time.

B. Speed/Path Tracking (SPT) Control Laws

The task of the TECS controller is decoupled speed and flight-path-angle tracking while providing adequate stability margin. These tasks are reflected by criteria that are computed from three nonlinear simulations and linear analysis; see Table 3. Simulations 1 and 2 are intended for flight-path angle and speed step-response shaping. Simulation 3 is intended to assess turbulence rejection. The corresponding scalings are given in Table 2. Those for damping and stability margins are as for the SCA criteria.

Of course, the SPT control laws always work via the SCA system. Thus, except for the TECS gains, also tuning parameters in the SCA controller affect the performance criteria in Table 3.

Table 3 Criteria for the SPT function[a]

Name	Description	Computation
Simulation 1, step: $\gamma_c = 3$ deg, no turbulence		
GArt	Rise time γ	see Note, Table 1
GAos	Overshoot γ	see Note, Table 1
GAst	Settling time γ	$\max_{t>25\,\mathrm{s}}\{\lvert\gamma_c - \gamma\rvert\}$
THcmd	θ cmd effort	$\max\{\lvert\dot{\theta}_c\rvert\}$
GAVA	max. speed deviation	$\max\{\lvert\Delta V_{\mathrm{cas}}\rvert\}$
Simulation 2, step: $V_c = 10$ m/s, $\gamma = -3$ deg, no turb.		
VArt	Rise time V_{cas}	see Note, Table 1
VAos	Overshoot V_{cas}	see Note, Table 1
VAst	Settling time V_{cas}	$\max_{t>25\,\mathrm{s}}\{\lvert V_c - \Delta V_{\mathrm{cas}}\rvert\}$
dTHR	Throttle activity	$\max\{\lvert\dot{\delta}_{\mathrm{TH1}_c}\rvert\}$
VAGA	Max. γ deviation	$\max\{\lvert\Delta\gamma\rvert\}$
Simulation 3, heavy turbulence: trimmed on glide slope, $V_{wind} = 15.4$ m/s		
NZturb	Load factor variation	$(1/60)\int_{t=0}^{t=60}\Delta n_z^2 dt$
THCturb	θ cmd effort	$(1/60)\int_{t=0}^{t=60}\Delta\theta_c^2 dt$
THRturb	Throttle activity	$(1/60)\int_{t=0}^{t=60}\Delta\delta_{\mathrm{TH}_c}^2 dt$
Linear analysis		
gmAD	GM δ_E-act.	see Note, Table 1
pmAD	PM δ_E-act.	see Note, Table 1
gmSG	GM at γ-sens.	see Note, Table 1
pmSG	PM at γ-sens.	see Note, Table 1
gmSV	GM at V_{cas}-sens.	see Note, Table 1
pmSV	PM at V_{cas}-sens.	see Note, Table 1
DAMP	min. damping	$\min_i\{\zeta_i\}$

[a]Δ denotes deviation from trimmed value.

Table 4 Criteria for the glide slope mode[a]

Name	Description	Computation
Nonlinear simulation, offset of 50 m above glide slope, aircraft trimmed parallel to the GS, no turbulence		
GSrt	Rise time	See Table 1 footnote
GSos	Overshoot	See Table 1 footnote
GSst	Settling time	$\max_{t>30\,\mathrm{s}}\{\lvert H_{\mathrm{offset}}\rvert\}$
Monte Carlo simulations, all effects (e.g., turbulence, nonlinearities) included		
maxGLDdev	Max. abs. vertical deviation from GS	$\max_{i_{\mathrm{mc}}}\{\max_{10\,\mathrm{s}<t<t_{\mathrm{fl}}}\{\lvert\epsilon_{\mathrm{GS}}(t)\rvert\}\}$
maxGLDdev50	Abs. vert. dev. from GS, at flare init	$\max_{i_{\mathrm{mc}}}\{\lvert\epsilon_{\mathrm{GS}}(t_{\mathrm{fl}_{i\mathrm{MC}}})\rvert\}\}$
meanGLDdev	Mean deviation from GS	$\sum_{i=1}^{n_{\mathrm{mc}}}\int_{t=10}^{t_{\mathrm{fl}_{i\mathrm{MC}}}}\epsilon_{\mathrm{GS}}(t)dt/\cdots$ $\sum_{i=1}^{n_{\mathrm{mc}}}(t_{\mathrm{fl}_{i\mathrm{MC}}} - 10)$
maxTHEdev	Max pitch angle dev. from mean value	$\max_{i_{\mathrm{mc}}}\{\max_{10\,\mathrm{s}<t<t_{\mathrm{fl}}}\{\lvert\theta(t) - \bar{\theta}\rvert\}\}$
maxVCdev	Max. speed deviation	$\max_{i_{\mathrm{mc}}}\{\max_{10\,\mathrm{s}<t<t_{\mathrm{fl}}}\{\lvert V_{\mathrm{app}_{i\mathrm{MC}}} - V_{\mathrm{cas}_{\mathrm{filt}}} - 0.5\,\mathrm{m/s}\rvert\}\}$

[a]n_{mc} = total number of MC simulations, i_{mc} = index of individual MC simulation, $t_{\mathrm{fl}_{i\mathrm{MC}}}$ = flare initiation time for simulation i_{mc}, $\bar{\cdot}$ indicates mean value for $10\,\mathrm{s} < t < t_{\mathrm{fl}_{i\mathrm{MC}}}$, $V_{\mathrm{cas}_{\mathrm{filt}}}$ is V_{cas} filtered with 5-s time constant.

C. Glide Slope (GS) Mode

For the glide slope mode, again command shaping criteria are applied; see Table 4 (Nonlinear simulation). A more important aspect during glide slope and approach-speed tracking is disturbance rejection, whereas pitch attitude dynamics and throttle activity have to be limited for passenger comfort and pilot-acceptance reasons. Design requirements were based on indicators listed in the second column of Table 4. One possibility is to derive computational criteria from analytical covariance analysis. For this work, a different approach was tried, based on nonlinear approach and landing simulations

performed in online MC analysis that is used to compute statistical flare law criteria (discussed in the next subsection); see Table 4. Because each landing is performed with different parameter vectors $\boldsymbol{p}_e$ and $\boldsymbol{p}_a$, their variation is implicitly addressed in optimizing for disturbance rejection. Because of the large number of simulations involved, the risk that the optimizer may anticipate a specific noise signal is reduced. However, the random generators used in the MC analysis are reset before each run, so that the ith individual simulation in different MC runs always uses the same set of parameter values and noise signals. This is required to prevent noisy criteria resulting from variations in simulated disturbances. The scalings on the criteria are given in Table 2.

D. Flare Mode

For the flare mode, deterministic and stochastic criteria are considered. The deterministic criteria (Tables 2 and 5) are computed from a nonlinear landing simulation. The stochastic criteria are computed from online MC analysis. To this end, $n_{\mathrm{MC}} = 400$ nonlinear landing simulations are performed in which all disturbances are applied. Before each landing simulation i_{MC}, 16 operational parameters ($\in \boldsymbol{p}_a$, $\in \boldsymbol{p}_e$; see Fig. 1) are selected randomly, according to prescribed statistical properties. After completing the simulations, the mean values and standard deviations of so-called risk variables are determined. The longitudinal risk variables are the height of the main gear over the runway at 60 m from the threshold (HTP60) to assess the risk of short landings, the runway touchdown distance from threshold (XTD) to assess the risk of long landings, and the vertical speed with respect to the runway surface (VZTD) to assess hard landings. From the mean values and standard deviations, the distribution and cumulative distribution functions can be computed, assuming that these are Gaussian. Based on joint aviation requirements–all weather operations (JAR–AWO) specifications, each risk variable has a limit value for which the probability of exceedance must be proven to be less than 10^{-6} (average risk analysis).

For each of the risk variables, the mean value, standard deviation, and probability of exceeding the limit value are addressed via optimization criteria[4]; see Table 2. The probability criteria are addressed as illustrated in an example. The limit value for X_{TD} is 915 m. As optimization criterion, the actual value of X_{TD} for which the probability of exceeding equals 10^{-6} is taken:

$$X_{\mathrm{TD}_{lim,6}} : P\left(X_{\mathrm{TD}} \geq X_{\mathrm{TD}_{lim,6}}\right) = 10^{-6} \tag{6}$$

$X_{\mathrm{TD}_{lim,6}}$ is divided by its demanded value of 915 m and handled as an inequality constraint ($X_{\mathrm{TD}_{lim,6}}/915 < 1$). This is equivalent to demanding $P(X_{\mathrm{TD}} > 915) < 10^{-6}$. However, to achieve more margin (or lower probability of exceedance), the demanded value has been set to 680 m, or $X_{\mathrm{TD}_{lim,6}}/680\ \mathrm{m} < 1$, so that $P(X_{\mathrm{TD}} > 915) \ll 10^{-6}$. For certification, limit risks must also be computed. This involves repeated MC analyses where each time one model parameter is held fixed at one of its extreme values while other parameters vary as before. Compared with the standard analysis, the requirements on X_{TD} are hardly relieved. For this reason in the optimization an additional margin is aimed for by demanding a smaller limit value.

Table 5 Deterministic flare criteria: nonlinear simulation, no disturbances, nominal conditions[a]

Name	Description	Computation
XTDnom	Touchdown point	$x_{\mathrm{td}}(t_{\mathrm{td}})$
VZTDnom	Vert. touchdown speed	$\dot{H}_{\mathrm{ra}}(t_{\mathrm{td}})$
THgrad	$\dot{\theta}$ may not change sign	$1 - \min_{t_1 \leq t \leq t_{\mathrm{td}}}\{\dot{\theta}(t)\}$
dHgrad	$\dot{V}_Z$ may not change sign	$1 + \max_{t_1 \leq t \leq t_{\mathrm{td}}}\{\dot{V}_Z\}$
dDEmax	Elev. rate	$\max_{\mathrm{fl} \leq t \leq t_{\mathrm{td}}}\{\lvert\dot{\delta}_E\rvert\}$

[a] $t_{\mathrm{td}} =$ touchdown time, $t_1 =$ flare init time + 2 s.

VI. Controller Optimization Strategy

This section addresses step C in the design process in Fig. 2. For tuning the autopilot functions, the multiobjective optimization environment MOPS[3] is used. MOPS allows multiple optimization subtasks (setups), as defined in the previous section, to be comfortably combined into a single one. This feature allows for tuning controller functions simultaneously, as is described shortly.

In Sec. V, an optimization setup has been defined for each controller function. Optimizing each function independently does not guarantee sufficient performance of the complete system, because in spite of timescale separation between sequential loops, considerable dynamic interaction may be left. This especially holds for the SCA in combination with the flare and SPT functions. For this reason, the intention is to tune all controller functions simultaneously. However, to steer the optimization process in a structured way and to keep an overview over the large amount of criteria, simultaneous optimization is not performed in one shot. Instead, tuning is started with the SCA inner loop and then sequentially expanded with the problem setups for SPT and guidance functions. The tuning process is depicted in Fig. 7.

For a combined optimization task (step 1), criteria properties (scaling, type) are adjusted, and, if desired, multiple model cases are selected (step 2). The latter allows for compromising performance between nominal and worst-case model parameter combinations ($\boldsymbol{p}_e$, $\boldsymbol{p}_u$, and $\boldsymbol{p}_a$) and is therefore an effective means to address performance robustness.[3] After tuning and compromising via multiobjective optimization in step 3, performance and robustness of the resulting controller functions are assessed (step 4). After optimization or assessment, the designer may decide to adjust criteria scaling (loops 1, 2) to influence compromise solutions. In case of robustness problems, worst model cases may be added to the optimization (loop 2). In case the result is satisfactory, the next controller function setup is added (step 1). Eventually, all controller functions are optimized simultaneously.

As already mentioned, the SCA inner-loop function is tuned first. The linear controller parameters (K_θ and K_q) are used for command shaping. Because dynamic inversion is sensitive to modeling errors, special attention has to be paid to this issue.[9] For this reason, performance of the optimization result is evaluated for all combinations of extreme values of the longitudinal parameters in $\boldsymbol{p}_u$. If necessary, selected worst cases may be included in the optimization.

Next, the optimization setup for the TECS-based flight path and speed-tracking loop is added. The SCA setup is retained, but the criteria are changed into inequality constraints (step 2 in Fig. 7). During optimization the inner loop gains K_θ and K_q may thus be

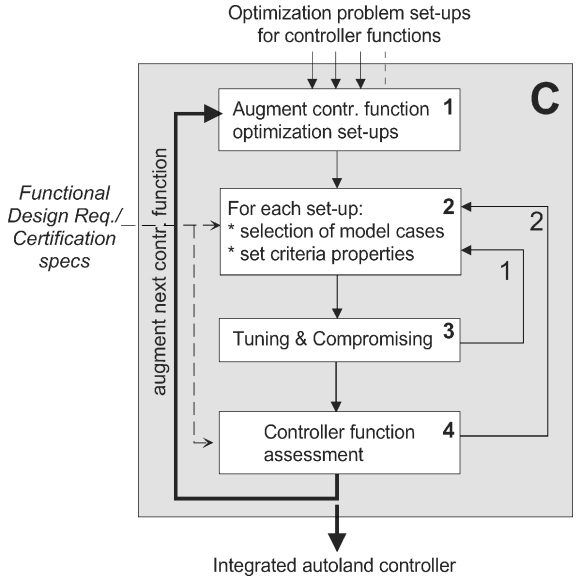

Fig. 7 Optimization-based autoland control laws design process (step C in Fig. 2).

adjusted to improve TECS performance, but the optimizer is prevented from distorting the achieved SCA performance by choosing gains K_θ and K_q that are only valid with TECS connected. Again, the newly optimized parameters are used as a start for the following step.

Next, the glide slope mode is added to the optimization. Criteria of the TECS setup are also set as inequality constraints. At this point, the MC-based criteria are left out, because their computation is too time consuming for an intermediate optimization step. During tuning of the glide slope mode, it became clear that tight path tracking could not be sufficiently achieved. Fortunately, in the TECS structure the gain K_F (normally 1) can be used to (temporarily) shift priority to flight-path tracking. Opening the speed loop (see Fig. 4) is also helpful. The parameter K_F may be adapted when the glide slope mode is connected. Evaluation of the criteria for TECS alone (as in the previous optimization) is performed for $K_F = 1$ and the speed loop is closed. Regarding tracking, the glide slope mode is most demanding. It is expected that other autopilot modes can be added later on, with no or only minor adjustment to TECS gains.

Finally, the flare mode is added, including MC-based criteria. Those related to the glide slope criteria are activated as well now (Table 4). The optimization task now includes all longitudinal autoland functions. All gains may be adjusted, and criteria from all subtasks (see Sec. VI) are active. Those in the SCA and TECS setups are set as inequality constraints. This on one hand allows these functions to be adjusted to improve outer-loop performance, but on the other hand prevents distortion of performance of the functions without the flare or GS mode connected.

VII. Formulation of the Basic Optimization Problem

For each design step, the problem of tuning and compromising (step 2 in Fig. 7) is formulated as a weighted min–max optimization problem, comprising all active criteria, over all subtasks (setups as defined in Sec. V), and over all selected model parameter cases per subtask:

$$\min_{T} \max_{ijk \in S_M} \{c_{ijk}(\boldsymbol{T}, \boldsymbol{p}_{ij})/d_{ijk}\}$$

$$c_{ijk}(T, p_{ij}) \le d_{ijk}, \qquad ijk \in S_I \tag{7}$$

$$c_{ijk}(T, p_{ij}) = d_{ijk}, \qquad ijk \in S_E$$

$$T_{\min,l} \le T_l \le T_{\max,l} \tag{8}$$

where S_M is the set of criteria to be minimized, S_I is the set of inequality constraints, and S_E is the set of equality constraints; $\boldsymbol{T}$ is a vector containing the tuning parameters T_l to be optimized, lying between the upper and lower bounds $T_{\max,l}$ and $T_{\min,l}$, respectively; $c_{ijk} \in S_m$ is the kth criterion of the jth model parameter case in the ith optimization subtask (e.g., flare, SCA) and d_{ijk} is the corresponding demand value, which serves as a criterion weight (Sec. V); and $\boldsymbol{p}_{ij}$ denotes a parameter vector of the ith subtask defining the jth model case. The criteria $c_{ijk} \in S_i$, S_e are used as inequality and equality constraints respectively. The affiliation of criteria to one of the groups (S_m, S_i, or S_e) can be changed at any time depending on the design progress. This feature is for example used when adding the TECS setup to the SCA one: the SCA criteria are changed from minimization to inequality constraints, allowing TECS performance to be improved while the demanded level of performance of the SCA function is allowed to deteriorate to the level of demanded criteria values (d_{ijk}). The optimization problem (7) is formulated automatically by the MOPS environment. Adding optimization subtasks or model cases and setting properties of criteria are done with the help of a graphical user interface or via scripts.[7]

The min–max optimization problem is solved by reformulating it as a standard nonlinear programming (NLP) problem with equality, inequality, and simple bound constraints. This reformulation is done fully automatically, after which the NLP problem is solved by using one of several available powerful solvers implementing local and global search strategies. Besides efficient gradient-based solvers, also gradient-free direct search-based solvers (usually more robust, but somewhat less efficient) are available to address problems with noisy or nonsmooth criteria. Solvers based on statistical methods or genetic algorithms are available as well. For this work, sequential quadratic programming (SQP) was used for the SCA and TECS functions, and a pattern search method was applied after augmenting the glide slope and flare setups, which turned out to cope better with the criteria derived from online MC analysis.

VIII. Controller Optimization Results

In this section the performance of the final controller (step D in Fig. 2) as well as intermediate results are assessed. Figure 8 shows the result of the optimization in so-called parallel coordinates. All scaled criterion values have been plotted on an individual axis and connected through a line (i.e., one graph corresponds to one tuning parameter set $\boldsymbol{T}$). The fat horizontal line indicates a value of one. Criteria values below this line are considered satisfactory. Parallel coordinates are standard graphical output during optimization with MOPS, giving quick insight into the optimization progress for criteria that are hard to satisfy and for criteria that conflict and thus have to be compromised.[3] The representation is used here to compare the intermediate optimization steps. Criteria vectors belonging to the different optimization setups have been separated by thick vertical lines.

The dash-dotted line (marker $\times$) in Fig. 8 represents the result after optimization of the SCA function. The other setups have not been involved yet, so that line can only be drawn for the SCA criteria. The resulting tuner parameter values can be found in the first column of Table 6. Because all scaled criterion values are below one, the result is satisfactory. The corresponding pitch attitude command response and the Nyquist curve for the loop opened at the elevator actuator have been plotted in Fig. 9 (dash-dotted curves). The phase margin is 85 deg, which is larger than the good-low value of 60 deg (Table 2) demanded for *pmAD*. As depicted in Fig. 8 on the *pmAD* axis, the scaled criterion value is thus 0 (note that this is the case for all linear criteria).

The result of the combined optimization of the SCA and SPT function is represented by the dashed line. This time, the curve can be drawn for the parallel coordinates up to *DAMP* (dashed line, marker o). The resulting tuning parameter values can be found in the second column of Table 6. All scaled criteria values are below one, except for *THcmd* and *THRturb* (set passive). However, exceedance with 20 and 40% was considered acceptable, because these criteria were not considered critical. Corresponding step responses on γ_a and V_{cas} can be found in Fig. 10 (dashed lines). Because of further adjustments to K_θ and K_q, SCA criteria values have changed in

Table 6 Development of tuner parameter values: augmented design setup (setup to the left is retained)[a]

Setup	Active tuner	SCA	TECS	GS	Flare	Unit
SCA	K_θ	1.6	2.0	2.0	2.1	s^{-2}
	K_q	2.5	3.2	3.2	3.3	s^{-1}
SPT (TECS)	K_{EI}		0.2	0.3	0.2	s^{-1}
	K_{TI}		0.4	0.3	0.43	s^{-1} rad^{-1}
	K_{EP}		0.56	0.4	0.33	——
	K_{TP}		0.6	1.0	1.2	rad^{-1}
	K_V		0.12	0.12	0.12	s^{-1}
	K_F		*1.0	1.0	0.28	——
	τ_V		*10	*10	8.8	s
GS	K_h			0.06	0.06	s^{-1}
	τ_h			2.5	2.6	s
	$\tau_{\dot{h}}$			15	3.9	s
Flare	K_{FL}				−0.04	rad $(m/s)^{-1}$
	H_{bias}				1.4	m
	$\dot{\theta}_{\text{Ramp}}$				0.18	rad/s
	K_{FW}				1	——
	K_{RW}				0.12	rad $(m/s)^{-1}$
	H_{retard}				6.0	m
	H_{flare}				12.1	m

[a]* = inactive.

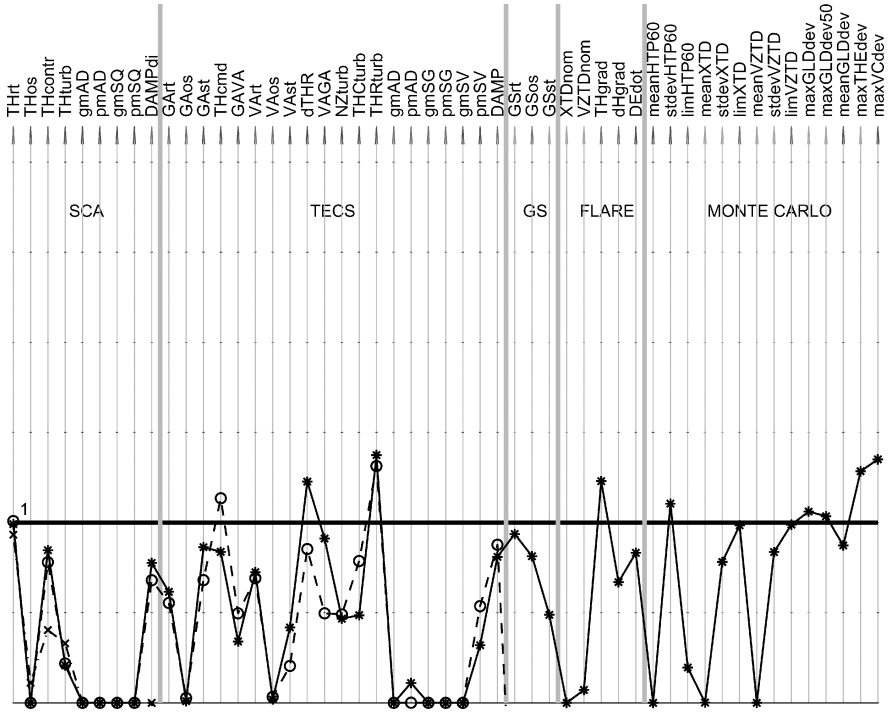

Fig. 8 Scaled criteria in parallel coordinates: —., SCA optim.; – – –, SCA+SPT optim.; ——, complete optimization. Scaled criteria values below the fat horizontal line satisfy demanded values.

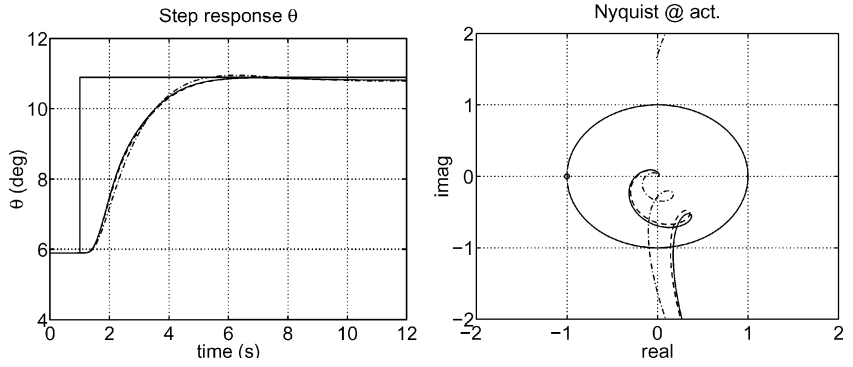

Fig. 9 SCA results: —., SCA optim.; – – –, SCA+SPT optim.; ——, complete optimization.

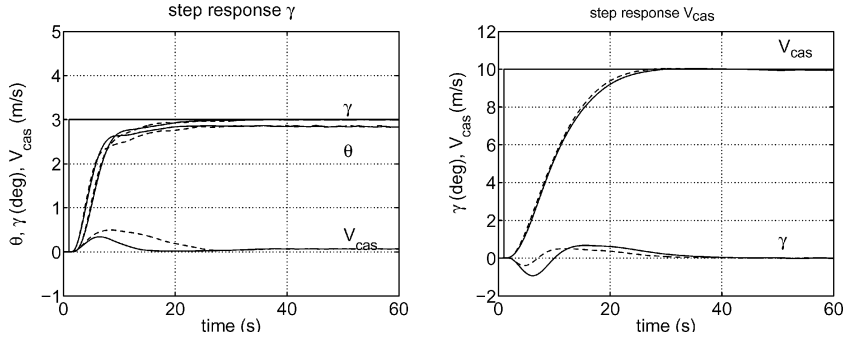

Fig. 10 TECS results: —., SCA optim.; – – –, SCA+SPT optim.; ——, complete optimization.

Fig. 8. *THrt* increased somewhat, but not beyond one (i.e., rise time <2.5 s), because the criterion was set as an inequality constraint in the optimization. Damping (*DAMPdi*) and control effort (*THcontr*) have deteriorated but are still acceptable (<1). Intermediate parameter studies with the SCA and TECS functions for longitudinal aerodynamic coefficients in $\boldsymbol{p}_u$ revealed that criteria values did not degrade to unacceptable levels. For this reason it was decided to proceed with the gains as found from optimization with the nominal aircraft model.

Results of the combined optimization of SCA, SPT, and GS setups are not discussed (third column of Table 6). The final optimization step involves all setups augmented into a single optimization task. The result is represented by a solid line in Fig. 8 (marker *). The corresponding tuner parameter values can be found in the fourth column of Table 6.

Regarding the nominal flare maneuver (Fig. 11), all criteria ($XTDnom \ldots DEdot$) are satisfactory, except for *THgrad* (Table 5). It turned out that a slight nose drop during the flare (0.3

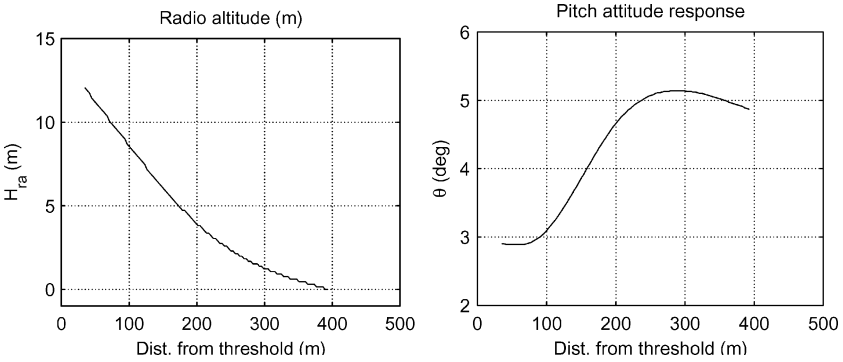

Fig. 11 Flare results.

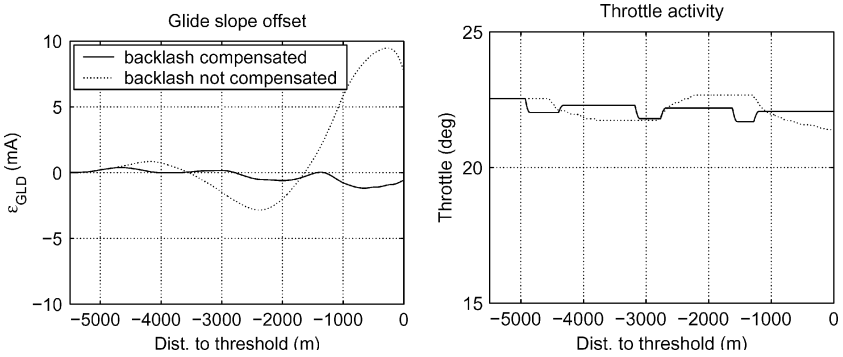

Fig. 12 Glide slope results.

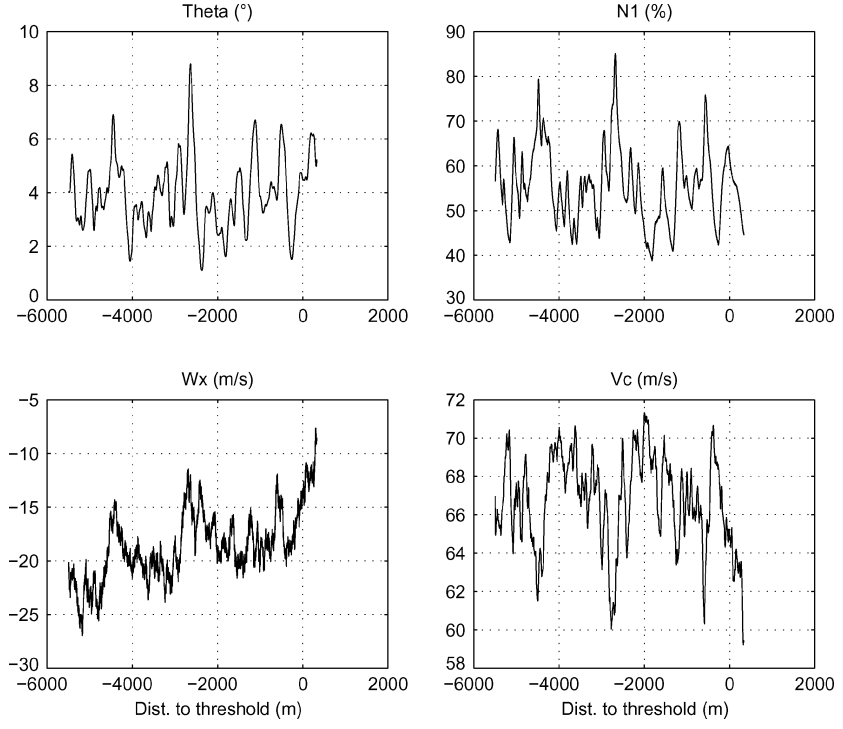

Fig. 13 Worst-case simulation from MC analysis.

deg) had to be tolerated, unless considerable emphasis was put on feedforward. However, this made it hard to meet MC assessment criteria, which will be discussed shortly. At this point, it became clear that architectural enhancements will be necessary to further improve the design.

A major concern for glide slope tracking was engine throttle backlash. Because TECS uses throttle for flight-path tracking, unacceptable oscillations arose. These could be reduced via a compensation scheme using measurement of the mean fan-shaft speed N_1 of both engines. Figure 12 shows nominal glide slope tracking performance and throttle activity without (dotted) and with backlash compensation (solid). Both throttle activity and oscillations have reduced considerably. The maximum overall deviation (*maxGLDdev*) and maximum deviation 50 m before threshold (*maxGLDdev50*) under turbulent conditions were difficult to improve beyond the criteria values shown in Fig. 8 (scalings had to be relieved as well; see Table 2). Inspection of individual landings from the MC analysis revealed that these maximum values occurred during extreme wind shears (>9 ft/s) caused by a combination of heavy turbulence and the standard wind profile as a function of height.[1] In further tuning, such cases should be eliminated. The TECS-related parameters have been considerably modified during the final optimization

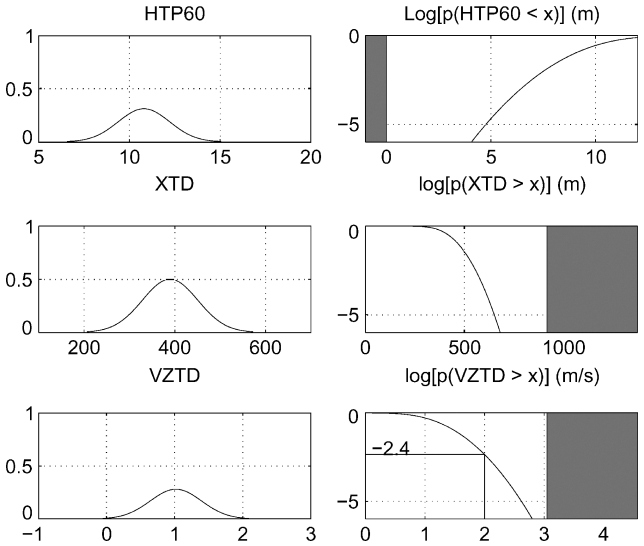

Fig. 14 MC simulation results.

step. Clearly, pitch attitude commands (*THcmd*) have decreased, at the cost of throttle activity (*dTHR*). This is related to minimizing pitch attitude excursions during glide slope tracking (*maxTHEdev*). However, the latter criterion was most difficult to improve. Again, it turned out that the maximum deviations occurred during heavy wind shears. Figure 13 shows an example simulation from MC analysis with a θ deviation of $\sim$5 deg resulting from a 3-s. wind shear of $\sim$9 ft/s. Regarding the SCA-related criteria, these slightly, but acceptably, deteriorate because of further adjustments of K_θ and K_q. The step response and Nyquist curve (solid) in Fig. 9 confirm this.

The most important criteria for certification are based on risk analysis from MC assessment. The optimized result can be found in Fig. 14. The left half of the figure shows distribution of the risk variables HTP60, XTD, and $VZTD$ computed from the mean and standard deviations from 2000 landings (during optimization, only 400 were used). To the right, the resulting cumulative distributions can be found. As an example for interpretation, the probability of landing at a sink rate (VZ_{TD}) higher than 2 m/s is $10^{-2.4}$, as indicated in Fig. 14. The graph should stay outside the shaded area, so that the probability of landing harder than 3 m/s (for ATTAS) is less than 10^{-6} (risk to be demonstrated). This has clearly been achieved by the optimizer. Incorporating these statistical criteria in the optimization was extremely useful because JAR–AWO robustness criteria could be addressed (and fulfilled) directly.

IX. Conclusions

The application of an optimization-based design process for automatic-landing control laws has been discussed.

Multiobjective optimization has proven to be very useful in handling the large number of design criteria. Design requirements regarding touchdown performance and glide slope tracking could be directly translated into numerical design criteria. For the SPA and SPT functions, standard step response criteria (computed from nonlinear simulations) and stability-related criteria such as damping and gain and phase margins have been successfully used.

It has further been demonstrated that robustness to varying (aircraft and environmental) parameters can be successfully addressed with the help of stochastic criteria computed from online Monte Carlo analysis. In the case of autoland, this implies that part of the certification criteria have been directly addressed in the optimization.

Final optimization of the system has been successfully performed for all functions simultaneously. This has been used to tune a single SCA function to work with the SPT and glide slope functions and with the flare law, as well as on its own. Optimization of the integrated system may thus help to reduce control-law complexity. However, to keep complexity of the optimization problem for the numerical algorithms and for the designer in hand, a stepwise tuning strategy has been proposed. After optimizing the SCA function, the outer-loop functions are sequentially added, allowing the designer to concentrate on one function at time but eventually resulting in optimization of all design parameters in the integrated system.

The design process resulted in good performance of the autoland system and, according to the MC analysis results, is able to cope well with varying aircraft and environment parameters. The flare law turned out to be close to its performance limits (e.g., a slight undesirable nose drop had to be accepted). For further improvement of performance and robustness, the structure may have to be enhanced.

The controller structure used in this design was successfully flight tested in September 2000 on DLR's ATTAS aircraft.[10]

Acknowledgments

This design is based on the autoland system that was developed by DLR within the project Robust and Efficient Autopilot Control Laws design (REAL), sponsored by the Commission of the European Community (Contract No. BRPR-CT-98-0627). The DLR design team consisted of Hans-Dieter Joos and Gertjan Looye (from the Institute of Robotics and Mechatronics, Oberpfaffenhofen) and Wulf Mönnich and Dehlia Willemsen (from the Institute of Flight Systems, Braunschweig). The MATLAB-based MC assessment tool, SIMPALE, was developed by project partner ONERA, France. Finally, the authors would thank the reviewers for their valuable comments.

References

[1]Joint Aviation Authorities Committee, "Joint Aviation Requirements, JAR–AWO All Weather Operations," Change 2, Global Engineering Documents, Engelwood, CO, Aug. 1996.

[2]Looye, G., Sancho, C., and Makdoembaks, A., "Design of Robust Autoland Control Laws Using μ-Synthesis," AIAA Paper 2002-4854, Aug. 2002.

[3]Joos, H.-D., "A Methodology for Multi-objective Design Assessment and Flight Control Synthesis Tuning," *Aerospace Science and Technology*, Vol. 3, No. 3, 1999, pp. 161–176.

[4]Looye, G., Joos, H.-D., and Willemsen, D., "Application of an Optimization-Based Design Process for Robust Autoland Control Laws," AIAA Paper 2001-4206, Aug. 2001.

[5]Schy, A. A., and Giesy, D. P., "Tradeoff Studies in Multiobjective Insensitive Design of Airplane Control Systems," AIAA Paper 83-2273, Aug. 1983.

[6]Kreisselmeier, G., and Steinhauser, R., "Systematische Auslegung von Reglern durch Optimierung eines vektoriellen Gütekriteriums," *Regelungstechnik*, Heft 3, 1979, pp. 76–79.

[7]Joos, H.-D., Bals, J., Looye, G., Schnepper, K., and Varga, A., "A Multiobjective Optimisation-Based Software Environment for Control Systems Design," *Proceedings of the IEEE International Symposium on Computer Aided Control System Design*, IEEE Publications, Piscataway, NJ, 2002, pp. 7–14.

[8]Tischler, M. B., Colbourne, J. D., Morel, M. R., Biezad, D. J., Cheung, K. K., Levine, W. S., and Moldoveanu, V., "A Multidisciplinary Flight Control Development Environment and Its Application to a Helicopter," *IEEE Control Systems Magazine*, Vol. 19, No. 4, 1999, pp. 22–33.

[9]Looye, G., "Design of Robust Autopilot Control Laws with Nonlinear Dynamic Inversion," *at–Automatisierungstechnik*, Vol. 49, No. 12, 2001, pp. 523–531.

[10]Bauschat, M., Mönnich, W., Willemsen, D., and Looye, G., "Flight Testing Robust Autoland Control Laws," AIAA Paper 2001-4208, Aug. 2001.

[11]Stevens, B. L., and Lewis, F. L., *Aircraft Control and Simulation*, Wiley, New York, 1992, Chaps. 1–2.

[12]Lambregts, A. A., "Integrated System Design for Flight and Propulsion Control Using Total Energy Principles," AIAA Paper 83-2561, Oct. 1983.

[13]Lambregts, A. A., "Vertical Flight Path and Speed Control Autopilot Design Using Total Energy Principles," AIAA Paper 83-2239, Aug. 1983.

[14]Enns, D. F., Bugajski, D. J., Hendrick, R. C., and Stein, G., "Dynamic Inversion: An Evolving Methodology for Flight Control Design," *International Journal of Control*, Vol. 59, No. 1, 1994, pp. 71–91.

[15]Lambregts, A. A., "Avoiding the Pitfalls in Automatic Landing Control System Design," AIAA Paper 82-1599, Aug. 1982.

[16]The Math Works Inc., *Control System Toolbox, For Use with MATLAB, User's Guide*, Natick, MA, Jan. 1998.